Pergamon

0042-6989(94)00254-1

Vision Res. Vol. 35, No. 12, pp. 1651–1666, 1995

0042-6989/95 $9.50 + 0.00

Underwater Refraction–Polarization Patterns of Skylight Perceived by Aquatic Animals Through Snell's Window of the Flat Water Surface

GÁBOR HORVÁTH,*† DEZSÖ VARJÚ*

Received 8 November 1993; in revised form 17 June 1994; in final form 7 October 1994

The grass shrimp (*Palaemonetes vulgaris*) orients itself by means of the polarization pattern of the sky visible through Snell's window of the water surface. The celestial polarization pattern viewed from water is distorted and modified because of refraction and repolarization of skylight at the air–water interface. This work provides a quantitative account of the repolarization of skylight transmitted through a flat water surface. The degree and direction of linear polarization, the transmissivity and the shape of the refraction–polarization oval are calculated at the air–water interface as functions of the polarization characteristics and the incident angle of partially linearly polarized incoming light. Two-dimensional patterns of linear polarization ellipses and of the degree and direction of polarization of skylight are presented for different zenith distances of the sun. The corresponding underwater refraction–polarization patterns are computed. Transmissivity patterns of a flat water surface are calculated for unpolarized light of an overcast sky and for partially polarized light of clear skies as a function of the zenith distance of the sun. The role of these refraction–polarization patterns in orientation and polarization vision of the grass shrimp (*P. vulgaris*) and rainbow trout (*Oncorhyncus mykiss*) is reviewed. The effects of cloud cover, surface waves and water turbidity on the refraction–polarization patterns are briefly discussed.

Refraction polarization of skylight Snell's window Underwater polarization vision Sun compass navigation *Palaemonetes vulgaris* *Oncorhyncus mykiss*

1. INTRODUCTION

The eyes of several terrestrial and semi-terrestrial species are sensitive to the plane of polarization of light. They can use the polarization of blue sky for sun compass navigation when the sun is occluded (Waterman, 1981). The situation is less clear in aquatic animals although many—e.g. Cladocera (Baylor & Smith, 1953), salmon (Groot, 1965), crab (Shaw, 1966), teleosts (Forward & Waterman, 1973), goldfish (Hawryshyn & McFarland, 1987)—can discriminate E-vector direction and perform polarotactic responses. Several functions have been proposed for underwater polarization sensitivity, including contrast enhancement of underwater objects against the background (Lythgoe & Hemmings, 1967), vertical migration (Umminger, 1968), maintenance of body position (Bardolph & Stavn, 1978) and goal-directed orientation (Waterman, 1988).

The optical properties of the air–water interface play an important role in the theory of radiative transfer in the earth's atmosphere (Coulson, 1988) and hydrosphere (Jerlov, 1976). Refraction of light is associated with polarization according to Fresnel formulae; unpolarized direct sunlight penetrating the water becomes partially linearly polarized. The pioneer measurements of Waterman (1954) demonstrated that underwater light is substantially polarized in all directions, mostly linearly but with some ellipticity just beyond the edge of Snell's window (Ivanoff & Waterman, 1958a).

From just under the water surface to a depth of about 50 m in the clearest water, the distribution and quality of light are strongly influenced by refraction. Through a flat water surface an aquatic animal sees the entire celestial over-water hemisphere condensed into Snell's window with an angular extent of 97 deg. Light from Snell's window in shallow waters contains most of the components of the spectrum available to terrestrial animals. Outside Snell's window the light from deeper layers is reflected, it is dim and its spectral range is restricted especially in open waters. At the boundary of Snell's window light from near the above-water horizon is split into a rainbow due to dispersion (Jerlov, 1976). An object above-water directly overhead suffers little

*Universität Tübingen, Lehrstuhl für Biokybernetik, Auf der Morgenstelle 28, D-72076 Tübingen 1, Germany.

†To whom all correspondences should be addressed at present address: Biophysics Group, Department of Atomic Physics, Loránd Eötvös University, H-1088 Budapest, Puskin u. 5–7, Hungary.

refractive distortion when seen from the water, but the image of objects near the horizon is substantially compressed (Horváth & Varjú, 1991). When the water is smooth, the boundary of Snell's window is sharp, and there is a strong contrast between the bright scene above and the darker reflections from deep water. Some plankton-feeding fishes living near the surface have an area of enhanced acuity on that part of their retinae where the boundary of Snell's window comes to lie (Munk, 1970). One of the two foveae of the compound eye in the water bug, *Notonecta glauca*, also looks in the direction of the edge of Snell's window when the animal is hanging below the water surface (Schwind, 1983, 1985).

There are two different underwater polarization patterns, one inside and one outside Snell's window. The celestial polarization pattern is present within Snell's window, but it is modified because of refraction and repolarization of skylight at the air–water interface. Further on in this work this pattern is called the refraction–polarization pattern (RPP) of skylight. Outside Snell's window is another polarization pattern, called the bulk transmission–polarization pattern (BTPP) created by interaction between water and sunlight transmitted. Both of these patterns vary with and contain information on the position of the sun. Earlier investigations on the RPP are lacking in the literature, while those of the BTPP are numerous (e.g. Kattawar, Plass & Guinn, 1973; Jerlov, 1976; Lundgren, 1976). The complex underwater intensity and polarization patterns (both RRP and BTPP) are modified by spatio-temporal variations of light distribution due to surface waves (Jelley, 1989). They focus sunlight at different depths depending on their wavelength; surface ripples focus light at depths of few centimetres, longer waves at greater depths (Schenck, 1957). Wave-focussing causes flicker, the frequency of which decreases with increasing depth.

All aspects of the underwater optical environment cannot be dealt with in a single paper since its mathematical treatment is very complex. Nevertheless, apart from the RPPs, the mathematics of radiative transfer in water is well established (Jerlov, 1976) and have been successfully applied to different aspects of underwater vision (Lythgoe, 1979; Pilgrim, Redfern, MacLachlan & Marsh, 1989). One of these aspects is the RPP, which however, to our knowledge has not been quantitatively investigated, although it plays an important role in orientation of some aquatic animals.

The number of aquatic animals which are known to use the RPP of skylight is relatively small. It has been demonstrated only recently that the grass shrimp (*Palaemonetes vulgaris*) orients by means of the RPP (Goddard & Forward, 1991). Other candidates for exploiting the RPP are migrating fishes. Rainbow trout (*Oncorhyncus mykiss*), for example, might also use RPP for sun compass orientation during migration (Hawryshyn, 1992). Certain water bugs, like *Corixa punctata* (Rensing & Bogenschütz, 1966) and *N. glauca* (Schwind, 1985) also possibly exploit the RPP. The RPP could also be of particular importance for orientation to other aquatic animals moving near the water surface, attracted to it by its higher oxygen content (Moyle & Cech, 1988) or driven there by predators (Schlosser, 1987).

The aim of this work is to calculate the RPP of the flat water surface. First, a quantitative account of the physics of repolarization of skylight transmitted through the water surface is given. The degree and direction of linear polarization, the transmissivity and the shape of the refraction–polarization oval are calculated at the air–water interface as functions of the polarization characteristics and the incident angle of partially linearly polarized incident light. Then two-dimensional patterns of linear polarization ellipses, and those of the degree and direction of polarization of skylight are presented for different zenith distances of the sun. The corresponding RPPs are computed. Transmissivity patterns are calculated for unpolarized light of an overcast sky and for partially polarized light of clear skies as a function of the zenith distance of the sun. The role of these RPPs for orientation in the grass shrimp (*P. vulgaris*) and rainbow trout (*O. mykiss*) is briefly reviewed. We confine our investigation to the flat water surface, because it is unimaginably complex to consider all possible surface disturbances (e.g. ripples). However, our calculations might be instructive as a first-order approximation of the real RPPs. The effects of cloud cover, surface waves and water turbidity on the RPPs are qualitatively and briefly discussed.

2. METHODS

The amplitude E_r and the direction φ_r of the refracted electric field vector and the transmissivity T of the air–water interface are given in Appendix A as functions of the incident angle θ_i and angle of obliqueness φ_i. The degree δ_r of linear polarization of refracted light and the transmissivity of the water surface are given in Appendix B for unpolarized incident light. In Appendix C the refraction polarization features of the air–water interface are derived for partially linearly polarized incoming light. The polarization characteristics of skylight were described by the semi-empirical Rayleigh model (Coulson, 1988; Schwind & Horváth, 1993; Horváth, 1995), which can be considered a good approximation for biological purposes (Waterman, 1981; Wehner, 1989). The light radiated by clouds of an overcast sky was assumed to be unpolarized.

The three-dimensional celestial hemisphere is represented in two dimensions in a polar-coordinate system. The angular distance θ from the zenith and φ from the solar meridian are measured radially and tangentially respectively. In this two-dimensional coordinate system the zenith is at the origin and the horizon corresponds to the outermost circle. To represent the RPP, a similar coordinate system parallel to the air–water interface is used. The boundary of Snell's window extends up to

$$\beta_{SW} = \arctan(n_a/\sqrt{n_w^2 - n_a^2}) = 48.5 \text{ deg}$$

measured from the zenith, where $n_a = 1.000$ and $n_w = 1.333$ are the refractive indices of air and water. Due to refraction the over-water world visible through the Snell's window is distorted (Horváth & Varjú, 1991): a point of the firmament with a zenith distance β is apparently seen in direction

$$\beta' = \arctan(n_a \sin\beta / \sqrt{n_w^2 - n_a^2 \sin^2\beta})$$

from the vertical. The apparent horizon corresponds to the boundary of Snell's window. Two different ways of representation of polarization patterns are used. (i) Distribution of celestial linear polarization ellipses and refraction–polarization ovals (RPOs). [Their long axes represent the direction, and their eccentricity the degree of linear polarization (see e.g. Guether, 1990). One must not mistake the linear polarization ellipse and oval for the elliptical polarization of light!] (ii) The regions of the sky and those of Snell's window with different values of transmissivity, degree and direction of polarization are shaded by different colours. In the calculations it was assumed that the air–water interface is flat (without ripples) and the refraction polarization of light at the water surface is governed by the Fresnel formulae (Guenther, 1990). The contribution of underwater polarization of light to the RPP due to scattering was neglected. This approximation is reasonable if the underwater observer is near the water surface. The list of symbols used, their meanings and their reference numbers can be found in Appendix D.

3. RESULTS

3.1. Refraction–polarization ovals, degree and direction of polarization of refracted light

In Fig. 1 the amplitude transmission coefficients $\sigma_\parallel$ and $\sigma_\perp$ (Guenther, 1990) for parallel and perpendicularly polarized incident light are shown as a function of the incident angle θ_i at the air–water interface (Appendix A). The vertically polarized light is slightly less attenuated than the horizontally polarized light at all incident angles

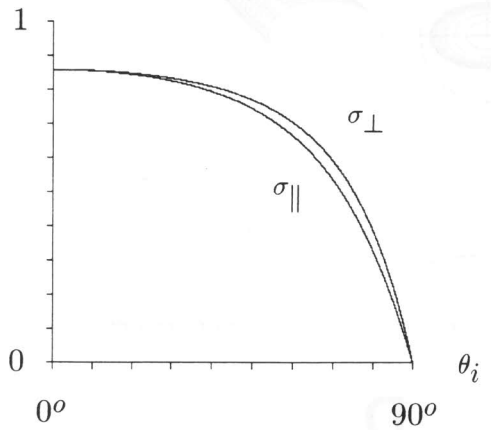

FIGURE 1. Amplitude transmission coefficients $\sigma_\parallel$ and $\sigma_\perp$ as a function of the incident angle θ_i (measured from the vertical) for parallel (with respect to the water surface) and perpendicular linear polarization of incoming light calculated for the air–water interface with $n_{air} = 1.000$ and $n_{water} = 1.333$.

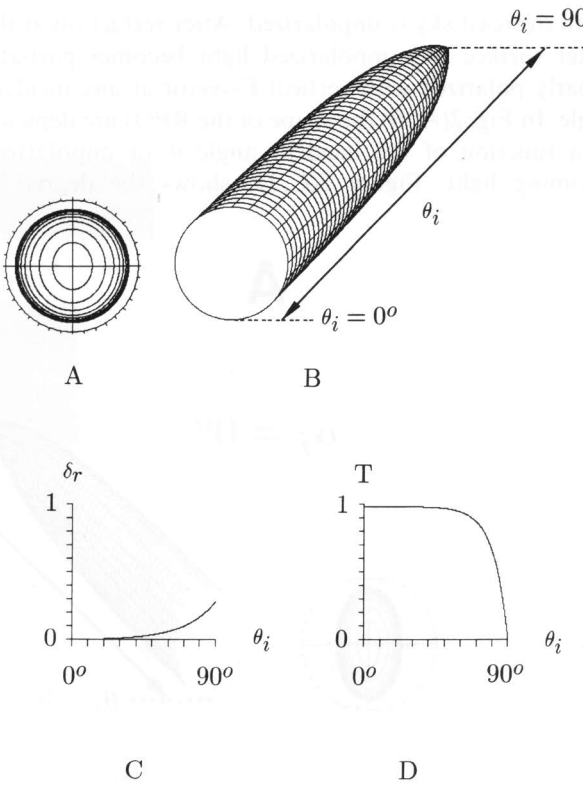

FIGURE 2. (A) RPOs for unpolarized ($\delta_i = 0$) incident light as a function of the incident angle θ_i increased from 0 to 90 deg in steps of $\Delta\theta_i = 9$ deg from the centre towards the periphery. The outermost circle (with a graduated scale) shows the spatial distribution of the electric field vector of unpolarized light. (B) Representation of the RPOs vs θ_i in a perspective plot. (C) Degree of linear polarization δ_r of refracted light, and (D) transmissivity T of the air–water interface vs incident angle θ_i of unpolarized incoming light.

θ_i except $\theta_i = 0$ deg and $\theta_i = 90$ deg. When the direction of the E-vector of totally polarized light is oblique, it can be decomposed into a horizontally and a vertically polarized component, both of which oscillate coherently. As the vertical component is less attenuated, the plane of polarization of the sum of the components will become more vertical, so that the E-vector rotates towards the vertical after refraction (if $\theta_i \neq 0$ deg and $\theta_i \neq 90$ deg).

The refractive indices of air and water varies slightly with the wavelength of light, so that less light is transmitted in the UV range of the spectrum than in the visible range (Guenther, 1990). This dispersion, however, is not strong. The refractive index of red light ($\lambda = 656.3$ nm) amounts to 1.3312, that of UV light ($\lambda = 308.2$ nm) to 1.3567. Therefore we omitted the spectral character of skylight and used in the calculations the refractive indices $n_{air} = 1.000$ and $n_{water} = 1.333$, that correspond to wavelengths in the middle range of the visible spectrum ($\lambda = 587.6$ nm). According to the field measurements by Ivanoff and Waterman (1958b) also, the effect of wavelength on underwater polarization is weak.

The light from the neutral Arago, Babinet and Brewster points of the firmament—positioned along the solar and anti-solar meridian, in the vicinity of the sun and anti-sun (Coulson, 1988)—and the diffuse light

of an overcast sky is unpolarized. After refraction at the water surface this unpolarized light becomes partially linearly polarized with vertical E-vector at any incident angle. In Fig. 2(A, B) the shape of the RPOs are depicted as a function of the incident angle θ_i of unpolarized incoming light. Figure 2(C, D) shows the degree of polarization δ_r of refracted light and the transmissivity T of the water surface for unpolarized incident light vs θ_i (Appendix B). As the incident angle increases, the size of the RPO decreases quasi exponentially [Fig. 2(A, B)] due to the decrease of the transmissivity [Fig. 2(D)]. Since $\sigma_\parallel \leqslant \sigma_\perp$ (Fig. 1) the RPO for unpolarized incident

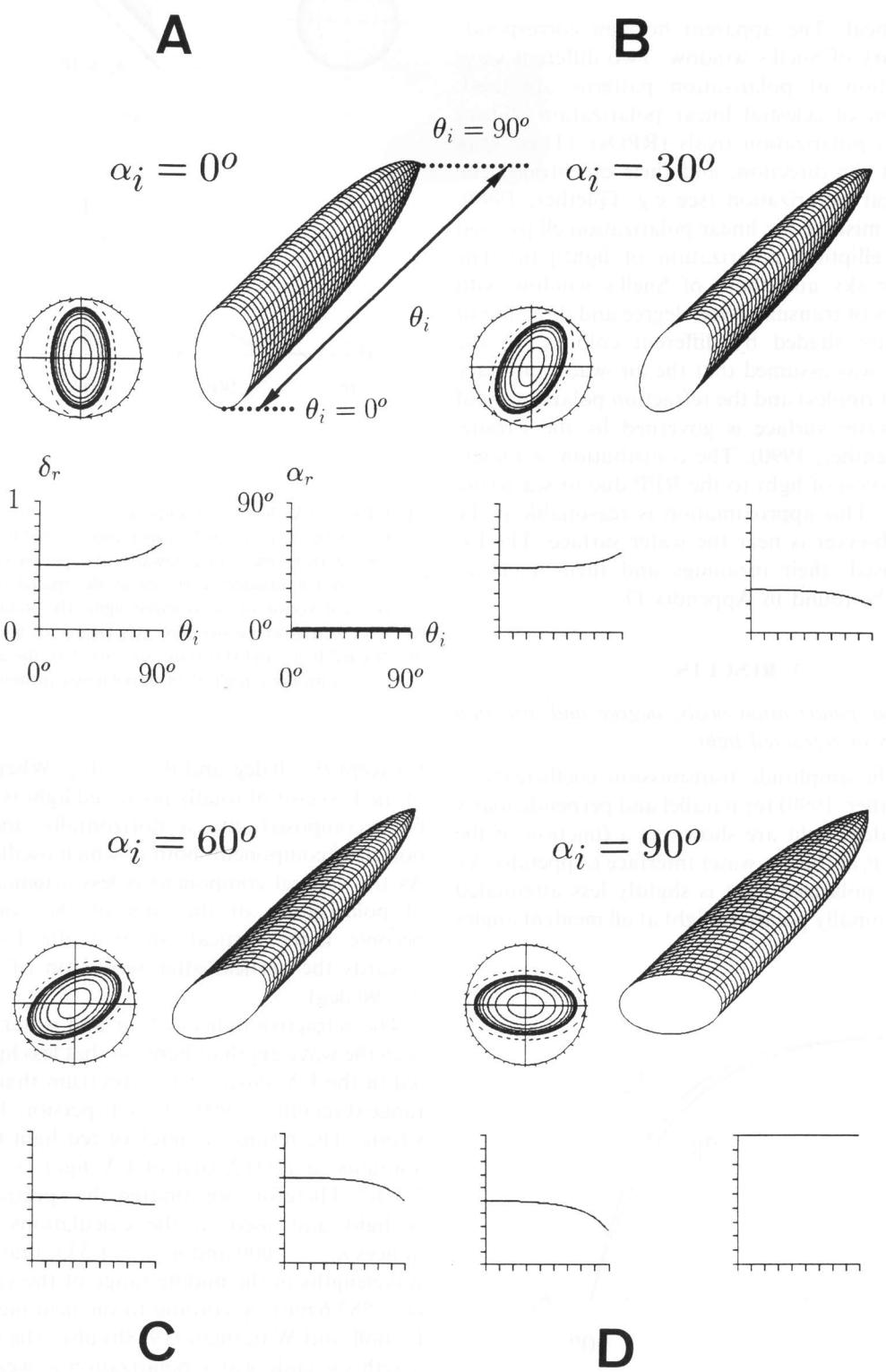

FIGURE 3. RPOs, degree δ_r and direction α_r of linear polarization of refracted light as a function of the incident angle θ_i of partially linearly polarized incident light with degree of polarization $\delta_i = 0.5$ for different values of the incident direction of polarization α_i measured from the vertical and given in the diagrams. The plots in (A)–(D) have the same meaning as the similar ones in Fig. 2. The dashed ellipses illustrate the polarization ellipses of incident light.

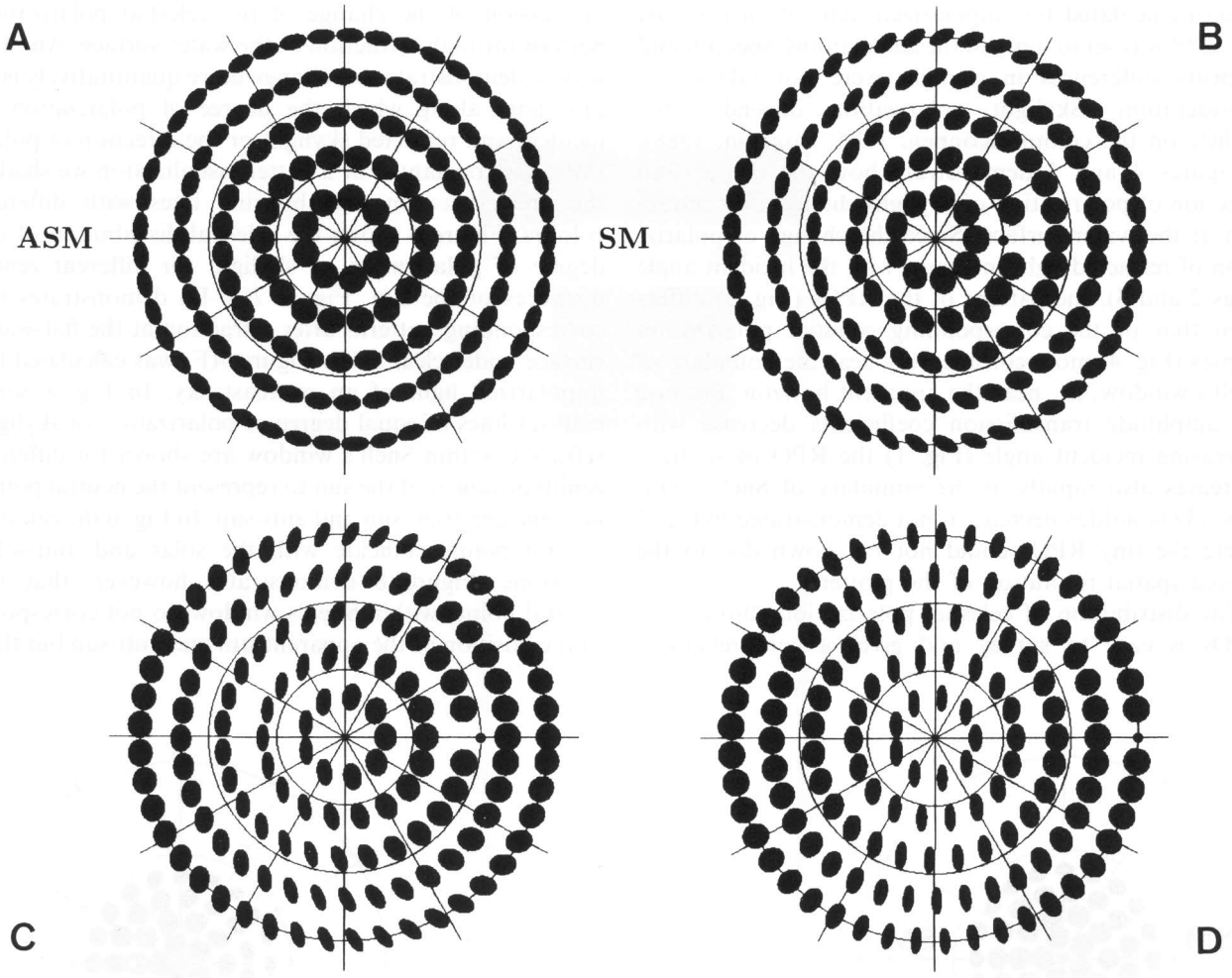

FIGURE 4. Two-dimensional representation of the pattern of polarization ellipses of skylight for different zenith distances θ_s of the sun (one must not mistake the linear polarization ellipse for the elliptical polarization of light!). The polar-coordinate system represents the celestial hemisphere. The zenith is at the centre, the sun is indicated by a dot, the horizon is the outermost circle; SM, solar meridian; ASM, anti-solar meridian. The direction of observation θ from the zenith is measured radially (zenith, $\theta_Z = 0$ deg horizon, $\theta_H = 90$ deg). The azimuthal angular distance φ is measured as the angle between the solar meridian SM and the meridian of the point observed (solar meridian, $\varphi_{SM} = 0$ deg; anti-solar meridian, $\varphi_{ASM} = 180$ deg). (A) $\theta_s = 0$ deg (sun at the zenith); (B) $\theta_s = 30$ deg; (C) $\theta_s = 60$ deg; (D) $\theta_s = 90$ deg (sun at the horizon).

light is slightly elongated [Fig. 2(A, B)]. The greater the incident angle, the larger the degree of polarization of refracted light [Fig. 2(C)].

If the incident light is partially linearly polarized—as is skylight—the spatial distribution of the incident E-vectors is characterized by a polarization ellipse. (The distribution of the refracted E-vectors is not described by an ellipse but by an oval.) In this case the effects of refraction on the unpolarized and totally polarized parts of incident light can be superimposed. The unpolarized component is partially converted into vertically polarized light (Fig. 2) and the totally polarized part rotates its plane of oscillation towards the vertical, unless its direction is horizontal or vertical. Figure 3 illustrates the RPOs, the degree δ_r and direction α_r of polarization of refracted light as a function of the incident angle θ_i for a given degree of polarization ($\delta_i = 0.5$) and for different directions of polarization α_i of partially linearly polarized incident light (Appendix C). Since the vertical component of the incident electric field vectors is less attenuated than the horizontal one (Fig. 1), the RPO rotates towards the vertical (i.e. α_r decreases) as the incident angle increases, whenever the incident E-vector is oblique relative to the water surface [Fig. 3(B, C)], but not when the incident E-vector is vertical [Fig. 3(A)] or horizontal [Fig. 3(D)]. Figure 3 also demonstrates that the degree of polarization δ_r of refracted light increases with increasing incident angle θ_i when α_i is <30 deg [Fig. 3(A, B)]. The opposite is true when α_i is >60 deg [Fig. 3(C, D)].

3.2. Refraction–polarization patterns of skylight visible through the Snell's window of flat-water as a function of the zenith distance of the sun

One of the possible ways of displaying the celestial polarization pattern is to represent the distribution of polarization ellipses of skylight in two dimensions. This is shown in Fig. 4 for four different zenith distances of the sun. Figure 5(A–D) shows the corresponding patterns of RPOs, and Fig. 5(E) the refraction–polarization

pattern calculated for unpolarized light of an overcast sky. E_i^{max} was set to unity in the calculations; spectral and intensity differences in skylight were not taken into consideration. Skylight polarization depends only slightly on the colour (Können, 1985; Coulson, 1988).

Figures 4 and 5 demonstrate how the degree and direction of polarization of skylight change after refraction at the water surface. Since the change of polarization of refracted light increases with the incident angle (Figs 2 and 3), the pattern of the RPOs (Fig. 5) differs from that of the corresponding celestial polarization ellipses (Fig. 4) more considerably near the boundary of Snell's window, i.e. near the apparent horizon. Because the amplitude transmission coefficients decrease with increasing incident angle (Fig. 1) the RPO of skylight decreases also rapidly at the boundary of Snell's window. (This sudden decrease is not demonstrated in Fig. 5 where the tiny RPOs could not be shown due to the limited spatial resolution of the plotter.)

The distribution of celestial polarization ellipses and RPOs is easy to survey and gives a comprehensive impression of the change of the celestial polarization pattern through refraction at the water surface. Another way to demonstrate this change more quantitatively is to plot lines along which the degree of polarization of incident and refracted skylight or the direction of polarization is constant. For a better visualization we shaded the areas between neighbouring lines with different colours. Figure 6 shows the celestial distribution of the degree of polarization of skylight for different zenith distances of the sun. Figure 7(A–D) demonstrates the corresponding patterns after refraction at the flat-water surface under clear skies. Figure 7(F) was calculated for unpolarized light of an overcast sky. In Fig. 8 some contour lines of equal degree of polarization of skylight refracted within Snell's window are shown for different zenith distances of the sun to represent the neutral points near the apparent sun and anti-sun. In Fig. 6 the celestial neutral points coincide with the solar and anti-solar positions. Figure 8 demonstrates however, that the neutral points within Snell's window do not correspond to the position of the apparent sun and anti-sun but they

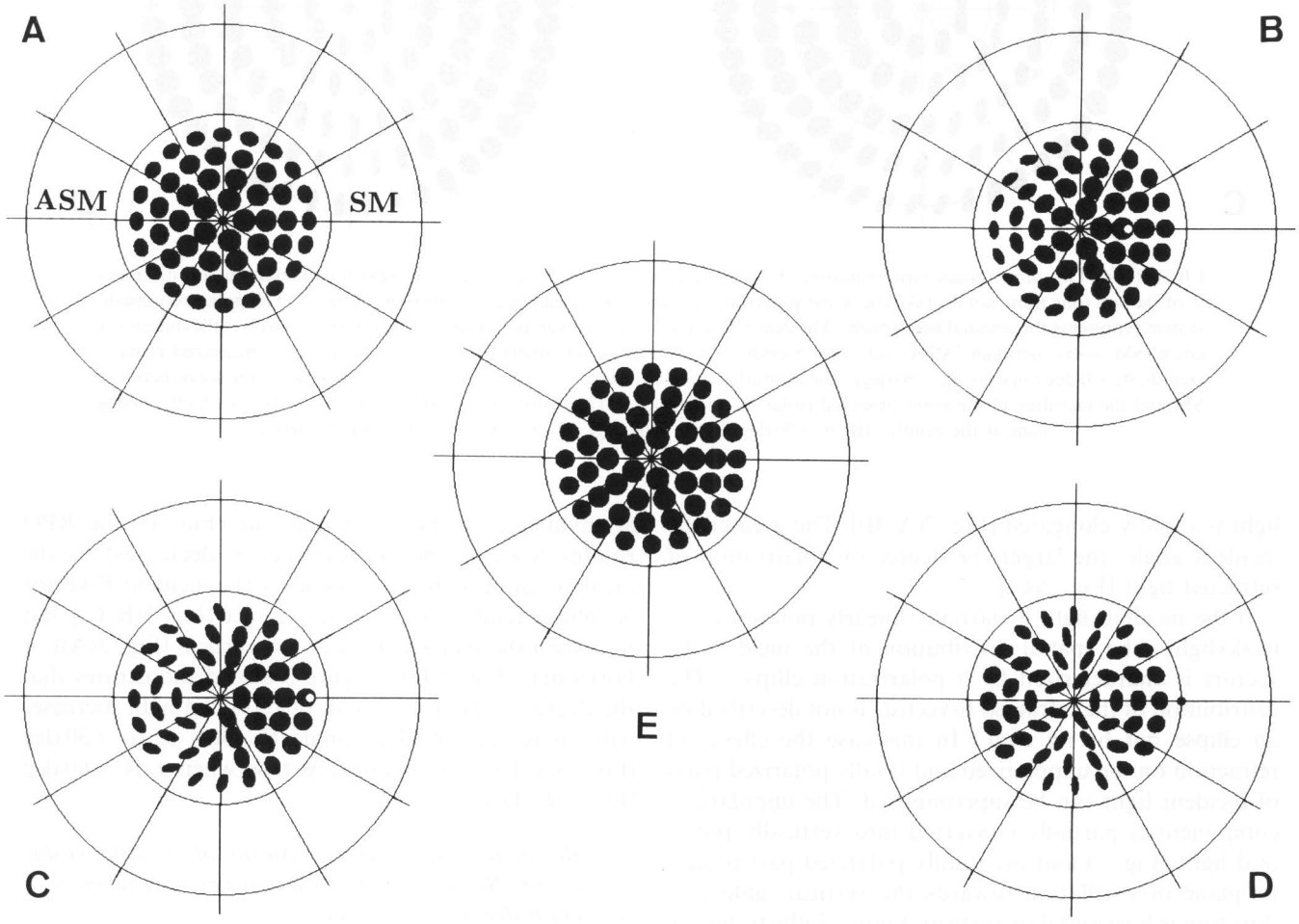

FIGURE 5. (A–D) Two-dimensional representation of the pattern of RPOs of skylight (one must not mistake the linear polarization oval for the elliptical polarization of light!) visible from water through the Snell's window of the flat water surface for different zenith distances θ_s of the sun and for the corresponding apparent zenith distances θ_s^a within Snell's window. (A) $\theta_s = 0$ deg, $\theta_s^a = 0$ deg; (B) $\theta_s = 30$ deg, $\theta_s^a = 22$ deg; (C) $\theta_s = 60$ deg, $\theta_s^a = 41.5$ deg; (D) $\theta_s = 90$ deg, $\theta_s^a = 48.5$ deg. The large circles correspond to the over-water horizon, the smaller ones represent the boundary of Snell's window with an angular diameter of 97 deg. Other conventions as in Fig. 4. (E) Pattern of the RPOs within Snell's window for unpolarized light of an overcast sky.

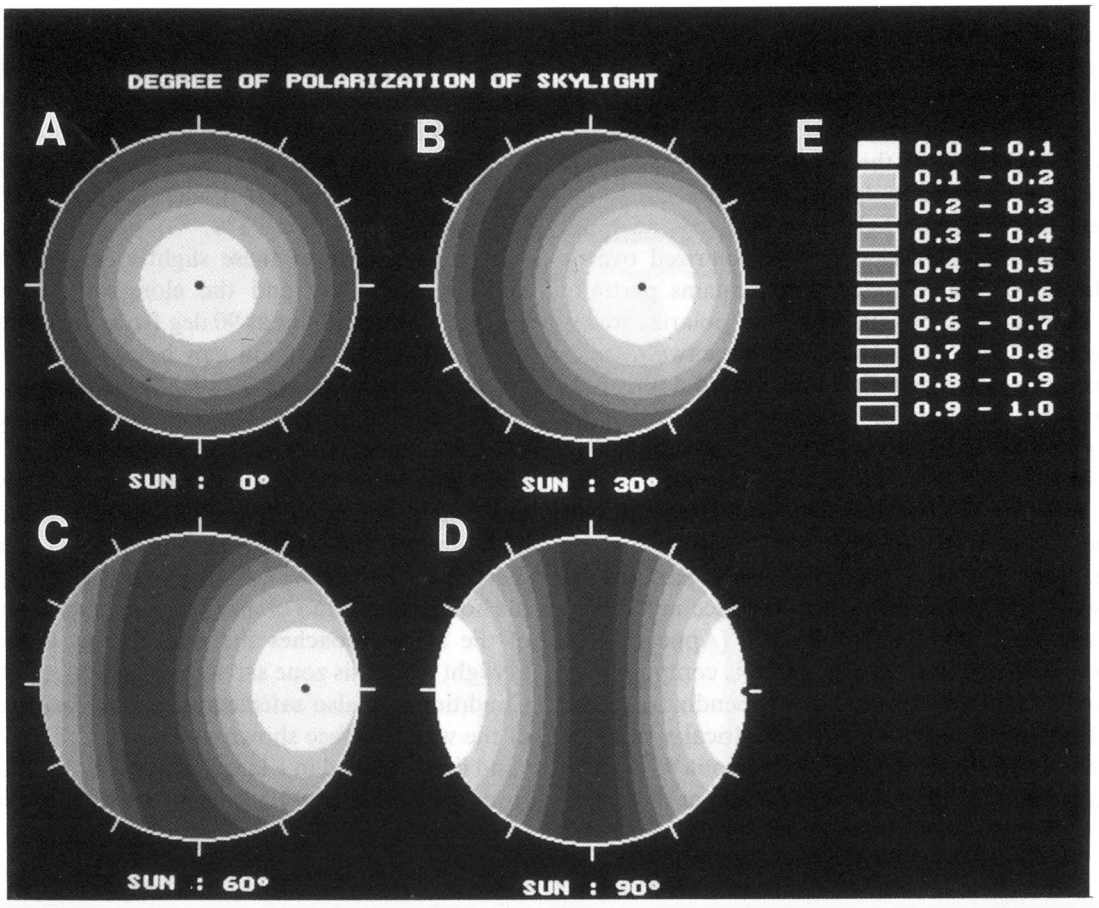

FIGURE 6. (A–D) Two-dimensional pattern of the degree of polarization of skylight for different zenith distances θ_s of the sun. Other conventions and parameters as in Fig. 4. (E) Colours corresponding to the different intervals of the degree of polarization ranging from 0 (white) to 1 (dark) in steps of 0.1.

are shifted further away from the latter, except when the sun is at the zenith [Fig. 8(A)].

In addition to the distortion of the contour lines of the degree of polarization by refraction, there are also some qualitative differences between the celestial polarization patterns in Fig. 6 and the corresponding RPPs in Figs 7 and 8. When the sun approaches the zenith the band of strongest polarization of the firmament with nearly horizontally polarized skylight lies near the horizon [Fig. 6(A, B)]. Since the degree of polarization of refracted light for nearly horizontally polarized incoming light decreases with increasing incident angle [Fig. 3(C, D)], the contour lines of equal degree of polarization of refracted light move further away from the solar point, i.e. they are shifted towards the boundary of Snell's window [Figs 7(A, B) and 8(A, B)]. However, when the sun approaches the horizon the celestial strongly polarized band with nearly vertically polarized skylight lies near the zenith [Fig. 6(C, D)]. Since the degree of polarization of refracted light for nearly vertically polarized incoming light increases with increasing incident angle [Fig. 3(A, B)], the contour lines of equal degree of polarization of refracted light are shifted towards the solar and anti-solar points [Figs 7(C, D) and 8(C, D)]. This results in two strongly polarized wedge-shaped patches near the boundary of Snell's window perpendicularly to the solar meridian [Figs 7(C, D) and 8(C, D)].

The patterns of the direction of polarization of skylight (the celestial E-vector distribution) are shown in Fig. 9 as a function of the zenith distance of the sun. Since all celestial E-vectors are directed horizontally when the sun is at the zenith, the pattern in Fig. 9(A) is uniformly dark. The corresponding patterns of refracted skylight are shown in Fig. 10. The refracted E-vector is also always horizontal when the sun is at the zenith, the pattern in Fig. 10(A) is, therefore, also homogeneously dark. In this two-dimensional representation the contour lines of equal direction of polarization in Fig. 9(B–D) converge. The centre of the convergence is called the focal point of the contour lines. One of the celestial focal points is always the zenith, and the other ones are the solar and anti-solar positions [Fig. 9(B–D)].

The most prominent difference between the patterns in Figs 9 and 10 is that the focal point at the sun [Fig. 9(B)] is split into two focal points positioned around the apparent sun along the solar meridian [Fig. 10(B)]. The skylight from the solar meridian is always horizontally polarized and its degree of polarization decreases gradually towards the sun, where it is

unpolarized. The unpolarized direct sunlight becomes slightly vertically polarized after refraction (Fig. 2). As the direction of view moves off the sun, the degree of polarization of skylight gradually increases along the solar meridian (Fig. 6). If the degree of polarization of this light is low, i.e. the angular distance from the sun is small, then the refracted light also becomes partially vertically polarized. However, if it is polarized over a certain threshold, the refracted light remains partially horizontally polarized but its degree of polarization is slightly reduced [Fig. 3(D)]. Hence there are two distinct points along the solar meridian and near the apparent sun where the direction of polarization of refracted skylight switches from vertical to horizontal. These points coincide with the two focal points around the apparent sun [Fig. 10(B)] and they constitute the two neutral points there [Fig. 8(B)].

In Fig. 11(A–D) the two-dimensional patterns of transmissivity of the flat air–water interface are shown for different zenith distances of the sun (Appendix C). The transmissivity pattern in Fig. 11(F) is computed for unpolarized light of an overcast sky (Appendix B). These patterns have in all cases a quasi cylindrical symmetry for transmissivity values smaller than about 95%. The pattern calculated for clear sky with the sun at the zenith [Fig. 11(A)] and that for unpolarized skylight [Fig. 11(F)] have an exact cylindrical symmetry. As the sun approaches the horizon the contour lines of equal transmissivity gradually become elongated, they are flattened perpendicularly to the solar meridian. The patches in Fig. 11(C, D) represent those regions where the transmissivity is >98%.

The occurrence of these slightly brighter patches of high transmissivity and the elongation of the transmissivity contour lines at 90 deg from the solar meridian for sun near the horizon can be explained as follows. Due to the relationship $T = 1 - R$ between transmissivity T and reflectivity R, which is the consequence of the conservation of energy, the transmissivity is very high when R is very low. The reflectivity is very low when (i) the degree of vertical polarization of incident light is high, and (ii) the incident angle is near or smaller than the Brewster angle $\theta_B = 53$ deg. As the sun approaches the horizon the band of maximum degree of polarization of the sky approaches the zenith (Figs 6 and 9). The skylight from this zone satisfies condition i. Furthermore Condition ii is also satisfied at the two brighter patches of the water surface shown in Fig. 11(C, D). Conditions i and ii are fulfilled in a larger angular interval (measured from the zenith) at 90 deg from the solar meridian than

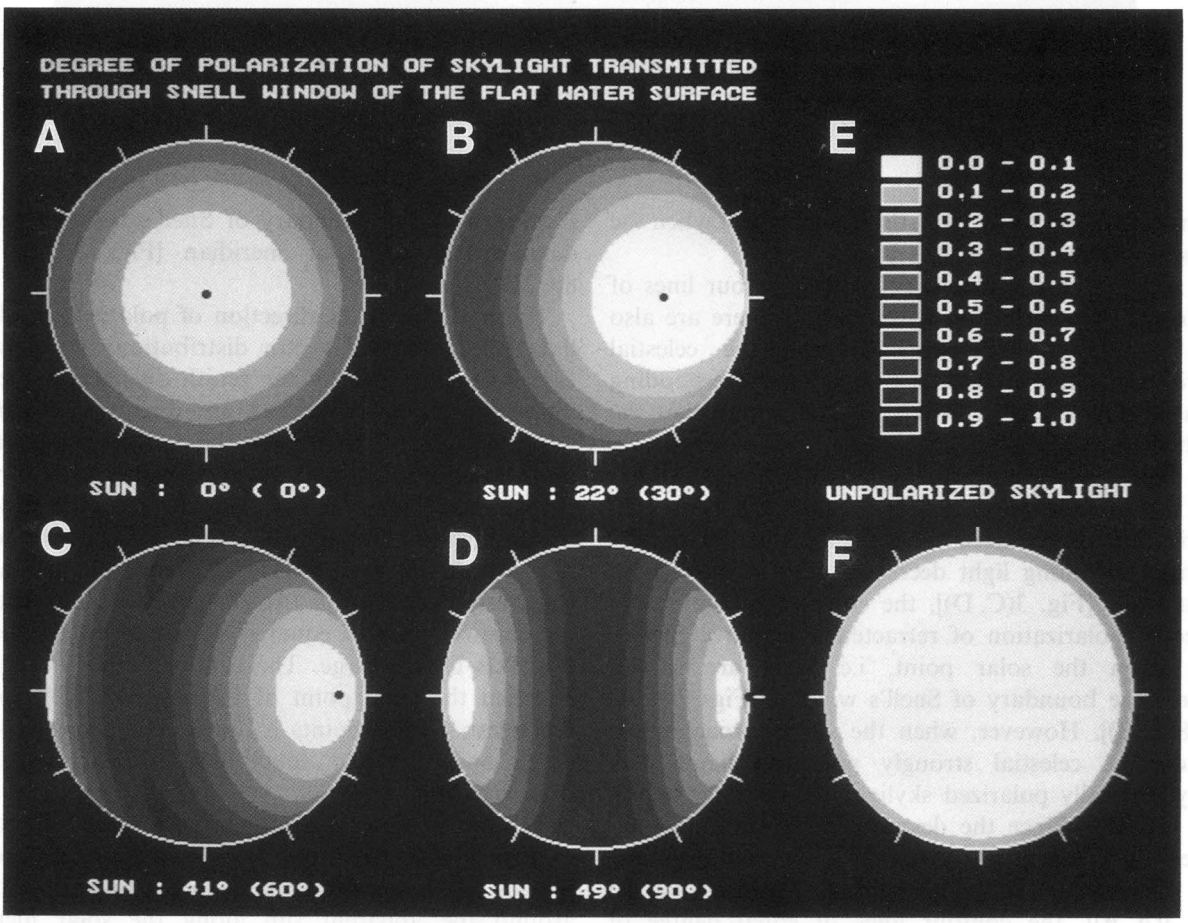

FIGURE 7. (A–D) Pattern of the degree of polarization of skylight refracted within Snell's window of the flat water surface under clear skies for different zenith distances θ_s of the sun and for the corresponding apparent zenith distances θ_s^a within Snell's window. θ_s and θ_s^a as in Fig. 5. (F) As (A)–(D) for unpolarized light of an overcast sky. The outermost circles represent the boundary of Snell's window. Other conventions as in Fig. 6.

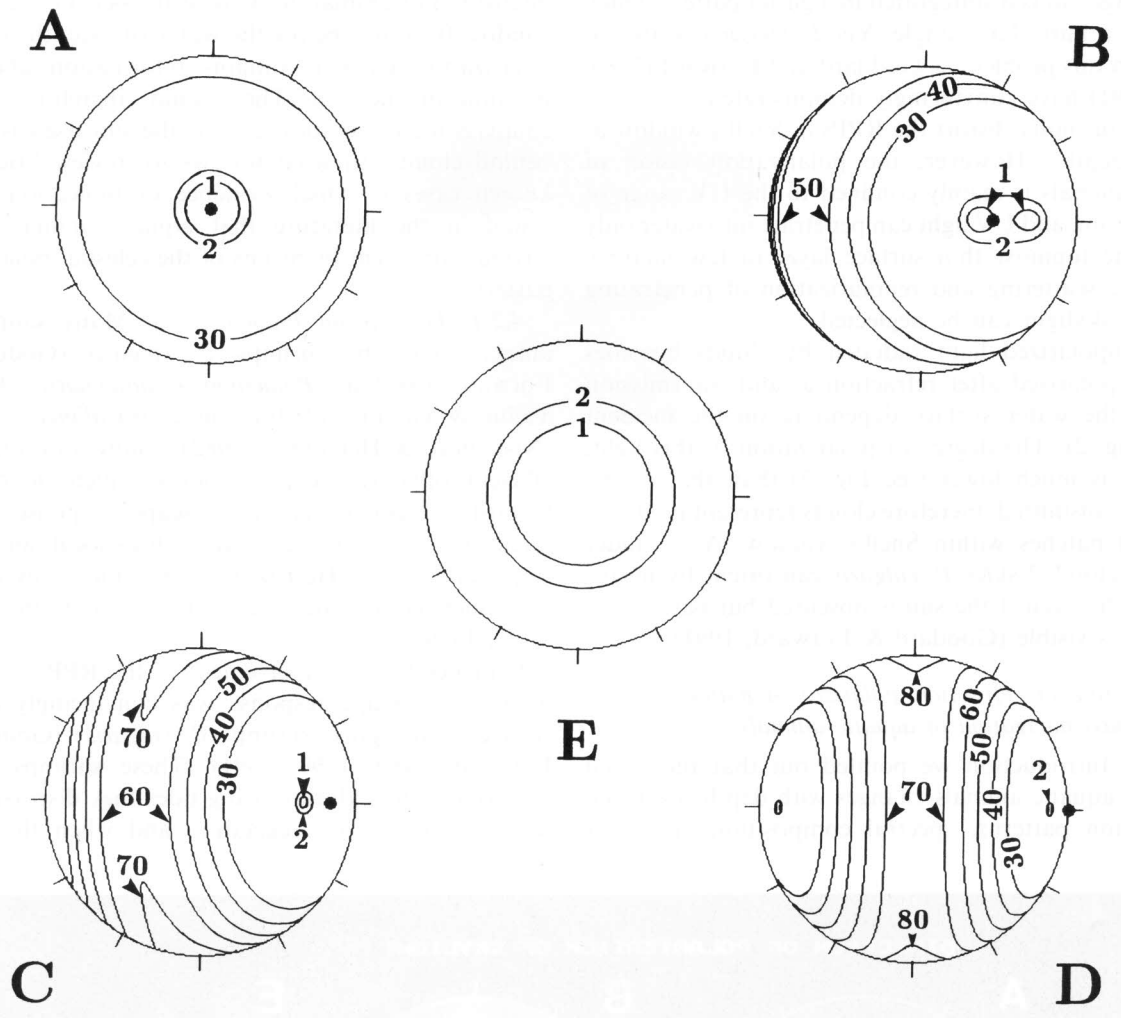

FIGURE 8. (A–D) Contour lines of equal degree of polarization of skylight refracted within Snell's window of the flat water surface for different zenith distances θ_s of the sun and for the corresponding apparent zenith distances θ_s^a within Snell's window, θ_s and θ_s^a as in Fig. 5. (E) As (A)–(D) for unpolarized light of an overcast sky. The apparent position of the sun is indicated by a dot; the outermost circles represent the boundary of Snell's window. The values of the degree of polarization of refracted light in per cent are indicated at the corresponding contour lines.

parallel to it. This results in the elongation of the transmissivity contour lines perpendicularly to the solar meridian [Fig. 11(C, D)]. For smaller zenith distances of the sun at least one of the above two conditions is not satisfied at any point of the water surface, so the brighter patches disappear [Fig. 11(A, B)]. These bright patches correspond to the two dark patches of the water surface visible from air, where the surface is particularly transparent (Können, 1985; Coulson, 1988; Schwind & Horváth, 1993; Horváth, 1995).

In Fig. 12(A, B) the region of the firmament is shown for two different zenith distances of the sun where the degree of polarization of skylight is $>65\%$. Figure 12(C, D) shows the corresponding regions within Snell's window. When the sun is hidden by clouds but the sky is visible, this region of the sky may contain some information for the sun compass orientation of rainbow trout in addition to the BTPP, since they are capable to orient by means of the underwater polarization of light, provided that the degree of polarization is $>65\%$ (Hawryshyn & Bolger, 1990).

4. DISCUSSION

4.1. The effects of surface waves, water turbidity and cloud cover on the refraction–polarization patterns

In the foregoing sections we have calculated so far the polarization pattern of refracted skylight immediately below the flat surface of calm waters [Figs 5, 7, 8, 10 and 12(C, D)], and the transmissivity of the flat air–water interface (Fig. 11). Ripples and waves not only act as optical lenses but also distort the RPP. In the open ocean, wind generated waves might have amplitudes of several metres and wavelengths up to a few hundred metres (Jelley, 1989). A simple calculation reveals that for a 10 m peak-to-peak amplitude and a 200 m wavelength, the maximum tilt of the water surface is 9 deg, which is the maximum refractive error of the estimated position of the sun. Marine animals might be able to navigate by means of the average position of the sun assessed through the RPP and integrated over time. The usefulness of the unobscured sun as an accurate compass is somewhat restricted by the fact that it seldom appears

as an image but is disintegrated in a glitter pattern which subtends a fairly large angle. Yet *P. vulgaris* is able to cope with this problem as Goddard and Forward (1989, 1990, 1991) have convincingly demonstrated.

Water turbidity distort the RPPs in Snell's window at greater depths. However, the polarization vision of aquatic animals is mainly confined to the UV range of the spectrum, and UV light can penetrate into water only within the topmost thin surface layer (a few metres), where the scattering and repolarization of penetrating refracted skylight can be neglected.

The unpolarized light radiated by clouds becomes partially polarized after refraction at and transmission through the water surface depending on the incident angle (Fig. 2). The degree of polarization of this light, however, is much lower (see Fig. 2) than that of the skylight transmitted, therefore clouds represent modestly polarized patches within Snell's window. Also, under partially clouded skies *P. vulgaris* can orient by means of the RPP, even if the sun is obscured but part of the blue sky is visible (Goddard & Forward, 1991).

4.2. The role of refraction–polarization patterns in the sun compass navigation of aquatic animals

In the Introduction we pointed out that the visual world of aquatic animals changes with depth regarding polarization patterns, spectral composition and light intensity. For animals looking at the sky through Snell's window from just below the water surface, the complex polarization pattern contains information about the position of the sun. They could, therefore use sun compass for orientation even if the sun itself is hidden behind clouds. In what follows we review briefly two known cases in which evidence or indication can be found in the literature that aquatic animals indeed navigate or orient by means of the celestial polarization pattern.

4.2.1. The shrimp Palaemonetes. Many shore-living animals—e.g. the shrimps *P. vulgaris* (Goddard & Forward, 1989) and *Palaemonetes antennarius* (Ugolini, Talluri & Vannini, 1989) or the crab *Callinectes sapidus* (Nishimoto & Herrnkind, 1982)—show an ecologically efficient offshore escape response which direct them towards deeper water. The escape response can be directed by cues on the shore such as local landmarks, slope, and waves (Herrnkind, 1983) and/or by celestial cues, such as the azimuthal position of the sun (Ugolini *et al.*, 1989).

Evidence for the involvement of the RPP of skylight in offshore escape response was convincingly demonstrated in the grass shrimp (*P. vulgaris*) (Goddard & Forward, 1989, 1990, 1991). These shrimps inhabit estuarine waters, during rising tides they disperse in the water-covered shore vegetation and when the tide is

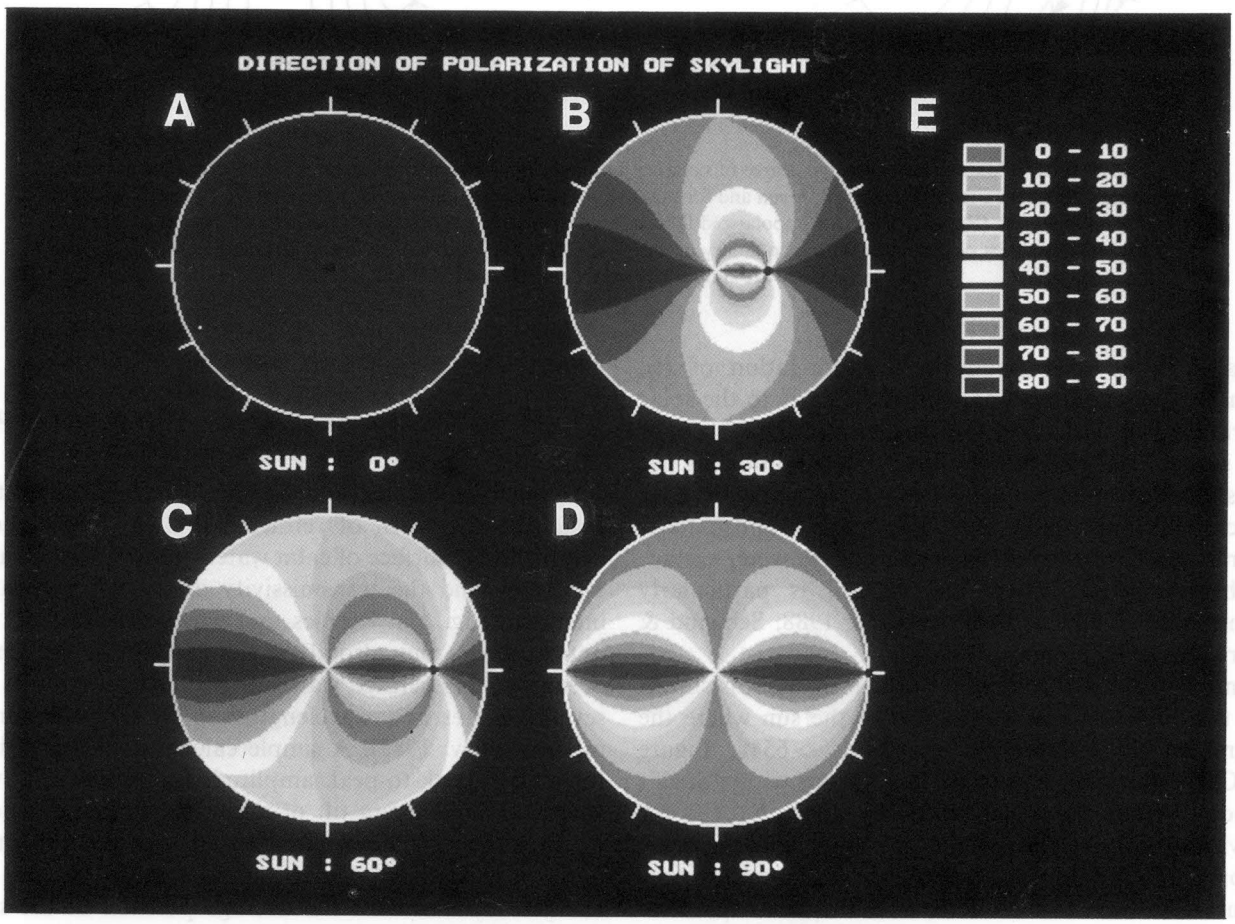

FIGURE 9. As Fig. 6 for the direction of polarization of skylight ranging from 0 (bright) and 90 deg (dark) in steps of 10 deg measured from the meridian of the point observed in the clear sky. Since all E-vectors of the celestial polarization pattern are horizontal when the sun is at the zenith, pattern (A) is homogeneously dark. Parameters as in Fig. 4.

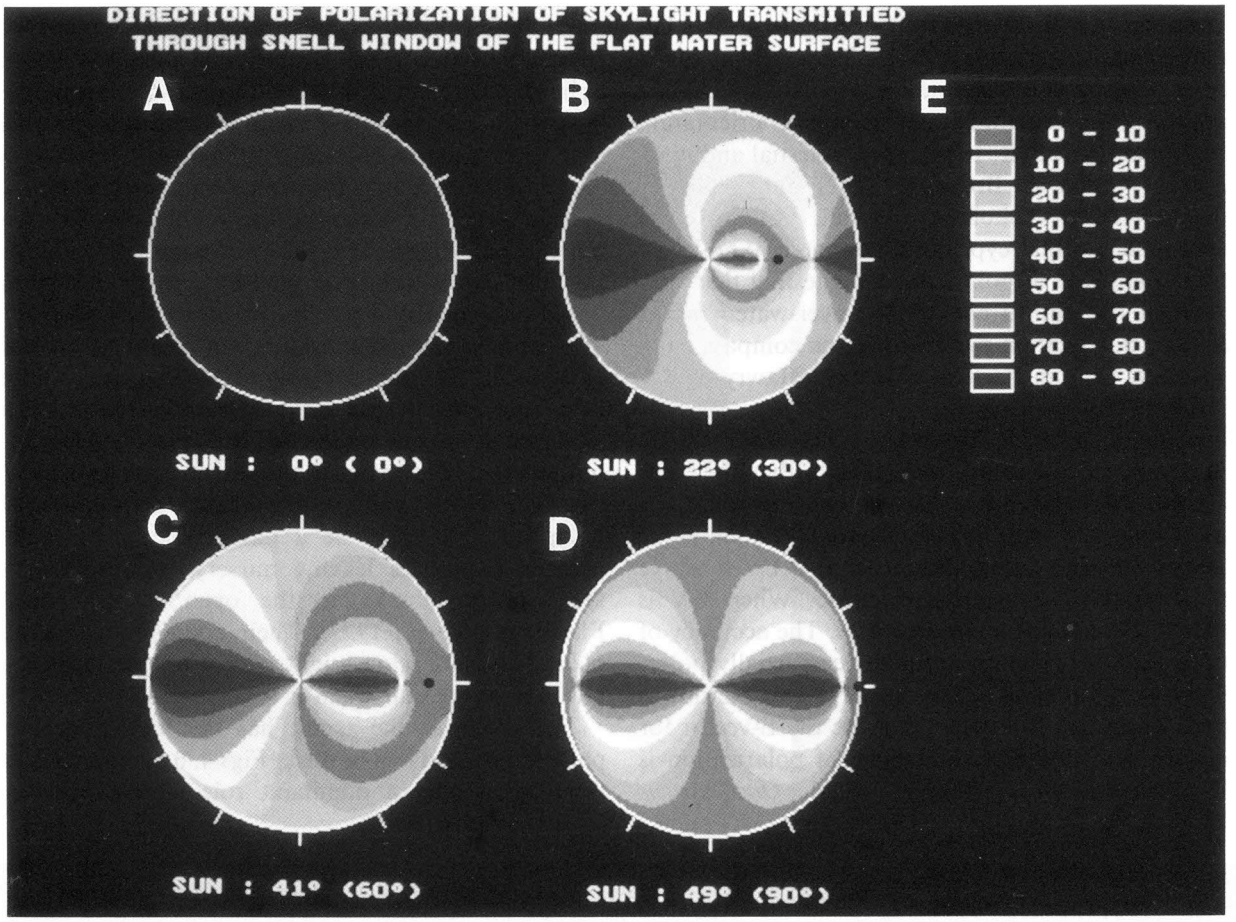

FIGURE 10. (A–D) Patterns of the direction of polarization of refracted skylight within Snell's window of the flat water surface under clear skies for different zenith distances of the sun. Since all refracted E-vectors are horizontal when the sun is at the zenith, pattern (A) is homogeneously dark. (E) Colours corresponding to the different intervals of the direction of polarization of refracted light ranging from 0 (bright) to 90 deg (dark) in steps of 10 deg measured from the meridian of the celestial point observed through the Snell's window. The outermost circles represent the boundary of Snell's window. Other conventions and parameters as in Fig. 7.

going out they retreat and congregate in shallow water near the shore. During low tide they are without sheltering vegetation, and therefore, vulnerable to shoreline predators. Most likely, *P. vulgaris* resembles its close relative *Palaemonetes pugio* (Douglas & Forward, 1989) and possesses eyes capable of perceiving polarized light. Ommatidia in this type of eye contain a rhabdom with two sets of microvilli, which are aligned orthogonally to each other.

Goddard and Forward (1989) found that *P. vulgaris* is capable of an offshore escape response when the sky is clear, or the sun can be seen through a clouded sky, or even if the sun is obscured but part of the blue sky is visible. This response is a time-compensated menotactic orientation that decays after 7–24 hr under constant conditions and overnight (Goddard & Forward, 1990). After extended periods of complete cloud cover and each morning after sunrise, the shrimp must relearn (within 2.5–4 hr) the relationship between the skylight cues and the offshore direction. There is a hierarchy of orientation cues: the sun can be used alone and is dominant over other celestial cues, and the polarization pattern of the sky is dominant over the intensity pattern. The polarization pattern is a backup cue for the position of the sun on partly cloudy days, when the sun is occluded but sky is visible; or on windy days, when ripples and waves would disintegrate the image of the sun while the polarization pattern remains relatively unaffected. Non-celestial cues would be essential on completely cloudy days or during the period of time when the shrimps are exploring a new shoreline (Goddard & Forward, 1990).

Orientation of *P. vulgaris* depends on the azimuth direction of the patch of blue sky viewed. When the patch is located within the solar hemisphere, the orientation of the shrimps is not significantly different from random. However, when the patch is in the anti-solar hemisphere, the shrimps are oriented in the correct offshore direction (Goddard & Forward, 1990). This may be explained by sky patches in the solar hemisphere having a much lower degree of polarization than those in the anti-solar hemisphere, particularly at high elevations of the sun (Figs 6–8 and 12).

4.2.2. Migrating fishes. Both Pacific and Atlantic salmonids migrate during a period of their life. Anadromous salmonids hatch and forage in the freshwater environment until they smolt, and thereafter they swim out to sea, where they spend a certain time in the open sea and return to their natal streams. The time of return

and distances travelled varies from species to species but the distances are thousands of miles (Hawryshyn, 1992). There is a variety of theories postulated to explain homing in fish, including sun compass orientation (Schwassmann & Hasler, 1964), other celestial and magnetic cues (Quinn & Brannon, 1982) and olfactory imprinting (Hasler, Scholz & Honrall, 1978). Recent evidence indicates that cyprinid fishes perceive both UV light and the plane of polarization suggesting that they may exploit the optical cues of the over-water and/or underwater polarization patterns for sun compass navigation when the sun itself is obscured (Hawryshyn & McFarland, 1987).

Hawryshyn, Arnold, Bowering and Cole (1990) demonstrated in laboratory experiments that the rainbow trout, *Oncorhyncus mykiss* is able to orient by means of polarized light. It is necessary to stimulate the blue-sensitive cones in addition to the UV-sensitive cones of trout to elicite this response. When UV is eliminated, E-vector orientation ceases. The accuracy of the orientation of rainbow trout under partially polarized light field decreases as the degree of polarization is reduced. Trout can still detect and use the E-vector for orientation provided that the degree of polarization is $>65\%$ (Hawryshyn & Bolger, 1990). *Oncorhyncus mykiss* loses the UV-sensitive cones during ontogeny and therefore its ability for orientation by means of polarized light (Hawryshyn, Arnold, Chiasson & Martin, 1989). Although light in the UV range is most strongly attenuated by water, Novales-Flamarique, Hendry and Hawryshyn (1992) demonstrated that there was enough light left near the water surface to stimulate all photoreceptors including the UV-sensitive ones in the retina of juvenile salmonides, even during crepuscular periods.

It is apparently only the juveniles that possess the ability to use UV polarized light for navigation, and they are actually migrating during this phase. Juvenile rainbow trout, for example, leave their native stream to enter a lake environment where they will spend their adult life until returning to spawn in the stream (Northcote, 1969). The UV vision and, in particular, detection of UV polarized light, may be a navigational tool used by juvenile salmonids leaving nursery lakes and coastal areas on their way to the open ocean (Novales-Flamarique *et al.*, 1992). Their ability to perceive the plane of polarization might play a role in locating the position of the sun when it is obscured.

The sky near the zenith has the highest degree of polarization at dawn or dusk [Figs 4, 6 and 12(A, B)] and thus might play a dominant role in fish orientation

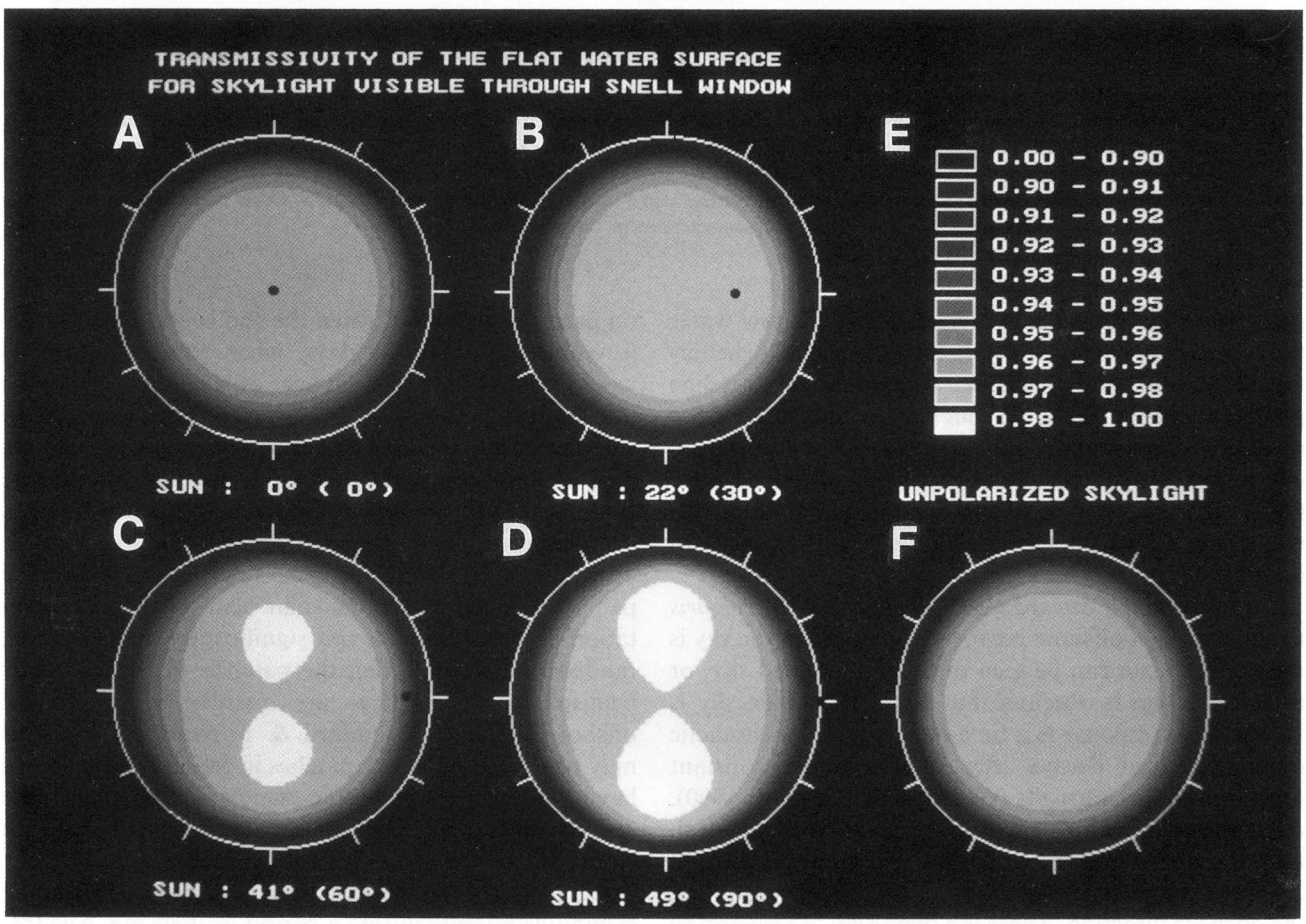

FIGURE 11. Patterns of the transmissivity of the flat air–water interface under clear skies visible from water through the Snell's window for different zenith distances of the sun. (E) Colours corresponding to the different intervals of the transmissivity ranging from 0.00 (dark) to 1.00 (white). (F) As (A)–(D) for unpolarized light of an overcast sky. In patterns (C) and (D) the two slightly brighter patches show the regions of Snell's window where the transmissivity is >0.98. The outermost circles represent the boundary of Snell's window. Other conventions and parameters as in Fig. 7.

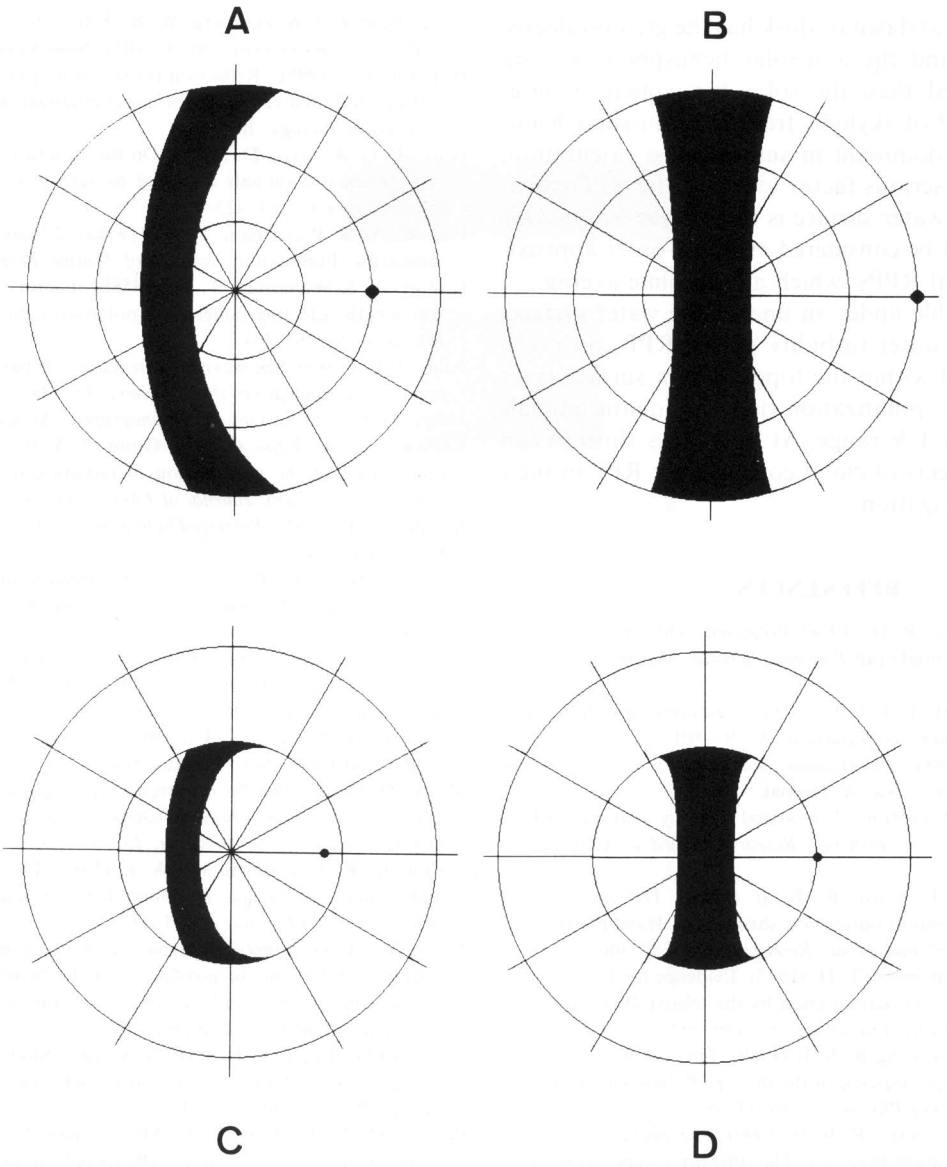

FIGURE 12. Top: regions of the firmament (black) where the degree of polarization of skylight is >65% for two different distances of the sun: (A) $\theta_s = 60$ deg; (B) $\theta_s = 90$ deg. Bottom: regions of Snell's window (black) where the degree of polarization of refracted skylight is over 65% for the corresponding two apparent zenith distances of the sun: (C) $\theta_s^a = 41$ deg; (D) $\theta_s^a = 48.5$ deg. The outermost circles in (A)–(D) represent the horizon, while the inner circles in (C) and (D) the boundary of Snell's window. The zenith is at the centre. The sun (A, B) and the apparent sun (C, D) are indicated by dots.

[Figs 5, 7, 8, 10, 11 and 12(C, D); Groot, 1965; Dill, 1971]. The results of Hawryshyn and Bolger (1990) however, support the conjecture that the rainbow trout is capable of orienting by means of less highly polarized light and, consequently, orientation is not necessarily restricted to dawn or twilight.

5. CONCLUSIONS

(i) The celestial polarization pattern viewed from water through the Snell's window of a flat air–water interface is modified through refraction and repolarization of skylight. At larger zenith distances of the sun there are two neutral points near the apparent sun along the solar meridian, and two strongly polarized patches near the boundary of Snell's window perpendicularly to the solar meridian. When the sun is near the zenith there is a neutral point above the apparent solar and anti-solar points near the boundary of Snell's window along the solar and anti-solar meridian. There are also two slightly brighter patches with high transmissivity values perpendicularly to the solar meridian.

(ii) The RPP of skylight appears to be an important visual cue for sun compass orientation of the grass shrimp (*P. vulgaris*). Also other shrimps might use this pattern for orientation. The rainbow trout (*O. mykiss*) and also other fish with polarization vision could exploit the RPP of the blue sky for sun compass navigation during migration. When the sun is near the horizon, the strongly polarized band of the sky might contain enough visual information for this task.

(iii) It has to be assumed that the accuracy of orientation in aquatic animals by means of polarization patterns is impaired when the degree of polarization is

reduced. The sky at dawn or dusk has the greatest degree of polarization and the anti-solar hemisphere is more strongly polarized than the solar hemisphere. Consequently, the RPP of skylight from the anti-solar hemisphere might be dominant in sun compass orientation.

(iv) The most serious factor affecting the RPP calculated for the flat-water surface is the surface waves. Our calculations must be considered as a first-order approximation of the real RPPs, which are the time average of the real ones visible under an undulating water surface. The influence of water turbidity on the RPP can probably be neglected within the topmost thin surface layer of seawater, where polarization vision of aquatic animals takes place in the UV range. At least grass shrimps can cope with the effects of cloud cover on the RPP in their sun compass navigation.

REFERENCES

Bardolph, M. & Stavn, R. H. (1978). Polarized light sensitivity in the stage I zoea of the mud crab *Panopeus herbstii*. *Marine Biology*, *46*, 327–334.

Baylor, E. R. & Smith, F. E. (1953). The orientation of Cladocera to polarized light. *American Naturalist*, *87*, 97–101.

Coulson, K. L. (1988). *Polarization and intensity of light in the atmosphere*. Hampton, Va: A. Deepak.

Dill, P. A. (1971). Perception of polarized light by yearling sockeye salmon. *Journal of the Fisheries Research Board of Canada*, *28*, 1319–1322.

Douglass, J. K. & Forward, R. B. Jr (1989). The ontogeny of facultative superposition optics in a shrimp eye: Hatching through metamorphosis. *Cell and Tissue Research*, *258*, 289–300.

Forward, R. B. & Waterman, T. H. (1973). Evidence for E-vector and light intensity pattern discrimination by the teleost *Dermogenys* sp. *Journal of Comparative Physiology*, *87*, 189–202.

Goddard, S. M. & Forward, R. B. Jr (1989). The use of celestial cues in the offshore escape response of the shrimp. *Palaemonetes vulgaris*. *Marine Behaviour and Physiology*, *16*, 11–18.

Goddard, S. M. & Forward, R. B. Jr (1990). The decay and learning of an y axis orientation behavior: The offshore escape response of the shrimp *Palaemonetes vulgaris* (Say). *Journal of Experimental Marine Biology and Ecology*, *142*, 137–150.

Goddard, S. M. & Forward, R. B. Jr (1991). The role of the underwater polarized light pattern, in sun compass navigation of the grass shrimp, *Palaemonetes vulgaris*. *Journal of Comparative Physiology A*, *169*, 479–491.

Groot, C. (1965). On the orientation of young sockeye salmon (*Oncorhyncus nerka*) during their seaward migration out of the lakes. *Behavior (Suppl.)*, *14*, 198.

Guenther, R. D. (1990). *Modern optics*. New York: Wiley.

Hasler, A. D., Scholz, A. T. & Horrall, R. M. (1978). Olfactory imprinting and homing in salmon. *American Scientists*, *66*, 347–355.

Hawryshyn, C. W. (1992). Polarization vision in fish. *American Scientist*, *80(2)*, 164–175.

Hawryshyn, C. W. & Bolger, A. E. (1990). Spatial orientation of trout to partially polarized light. *Journal of Comparative Physiology A*, *167*, 691–697.

Hawryshyn, C. W. & McFarland, W. N. (1987). Cone photoreceptor mechanisms and the detection of polarized light in fish. *Journal of Comparative Physiology A*, *160*, 459–465.

Hawryshyn, C. W., Arnold, M. G., Bowering, E. & Cole, R. L. (1990). Spatial orientation of rainbow trout to plane-polarized light: The ontogeny of E-vector discrimination and spectral sensitivity characteristics. *Journal of Comparative Physiology A*, *166*, 565–574.

Hawryshyn, C. W., Arnold, M. G., Chiasson, D. & Martin, P. C. (1989). The ontogeny of ultraviolet photosensitivity in rainbow trout (*Salmo gairdneri*). *Visual Neuroscience*, *2*, 247–254.

Herrnkind, W. F. (1983). Movement patterns and orientation. In Vernberg, F. J. & Vernberg, W. B. (Eds), *The biology of crustacea. 7. Behavior and ecology* (pp. 41–105). New York: Academic Press.

Horváth, G. (1995). Reflection-polarization patterns at flat water surfaces and their relevance for insect polarization vision. *Journal of Theoretical Biology*. In press.

Horváth, G. & Varjú, D. (1991). On the structure of the aerial visual field of aquatic animals distorted by refraction. *Bulletin of Mathematical Biology*, *53*, 425–441.

Ivanoff, A. & Waterman, T. H. (1958a). Elliptical polarization of submarine illumination. *Journal of Marine Research*, *16*, 255–282.

Ivanoff, A. & Waterman, T. H. (1958b). Factors, mainly depth and wavelength, affecting underwater polarized light. *Journal of Marine Research*, *16*, 283–307.

Jelley, J. V. (1989). Sea waves: Their nature, behaviour, and practical importance. *Endeavour (New Series)*, *13*, 148–156.

Jerlov, N. G. (1976). *Optical oceanography*. Amsterdam: Elsevier.

Kattawar, G. W., Plass, G. N. & Guinn, J. A. Jr (1973). Monte Carlo calculations of the polarization of radiation in the earth's atmosphere–ocean system. *Journal of Physical Oceanography*, *3*, 353–372.

Können, G. P. (1985). *Polarized light in nature*. Cambridge: Cambridge University Press.

Lundgren, B. (1976). Radiance and polarization measurements in the mediterranean. Internal report, University of Copenhagen, Copenhagen.

Lythgoe, J. N. (1979). *The ecology of vision*. Oxford: Clarendon Press.

Lythgoe, J. N. & Hemmings, C. C. (1967). Polarized light and underwater vision. *Nature*, *213*, 893–894.

Moyle, P. B. & Cech, J. J. (1988). *An introduction of icthyology*. Englewood Cliffs, N.J.: Prentice-Hall.

Munk, O. (1970). On the occurrence and significance of horizontal band-shaped retinal areas in teleosts. *Videnskabellae Meddelelser Danfra Naturhistorisk Forening*, *133*, 85–120.

Nishimoto, R. T. & Herrnkind, W. F. (1982). Orientation of the blue crab *Callinectes sapidus* Rathbun: Role of celestial cues. *Marine Behaviour and Physiology*, *9*, 1–11.

Northcote, T. G. (1969). Patterns and mechanisms in the lakeward migratory behaviour of juvenile trout. In Northcote, T. G. (Ed.), *Symposium on salmon and trout in streams* (pp. 183–203). Vancouver: University of British Columbia.

Novales-Flamarique, I., Hendry, A. & Hawryshyn, C. W. (1992). The photic environment of a salmonid nursery lake. *Journal of Experimental Biology*, *169*, 121–141.

Pilgrim, D. A., Redfern, T. A., MacLachlan, G. S. & Marsh, R. I. (1989). Estimation of optical coefficients from diver observations of visibility. *Progress in Underwater Science*, *14*, 33–52.

Quinn, T. P. & Brannon, E. L. (1982). The use of celestial cues and magnetic cues by orienting sockeye smolts. *Journal of Comparative Physiology A*, *147*, 547–552.

Rensing, L. & Bogenschütz, H. (1966). Vorzugsrichtungen von *Corixa punctata* Illig. in polarisiertem Licht. *Zoologischer Jahrbuch der Physiologie*, *72*, 123–135.

Schenck, H. (1957). On the focusing of sunlight by ocean waves. *Journal of the Optical Society of America*, *47*, 653–657.

Schlosser, I. J. (1987). The role of predation in age- and size-related habitat use by stream fishes. *Ecology*, *68*, 651–659.

Schwassmann, H. O. & Hasler, A. D. (1964). The role of the sun's altitude in the sun orientation of fish. *Physiological Zoology*, *37*, 163–178.

Schwind, R. (1983). Zonation of the optical environment and zonation in the rhabdom structure within the eye of the backswimmer, *Notonecta glauca*. *Cell and Tissue Research*, *232*, 53–63.

Schwind, R. (1985). Sehen unter und über Wasser, Sehen von Wasser: Das Sehsystem eines Wasserinsektes. *Naturwissenschaften*, *72*, 343–352.

Schwind, R. & Horváth, G. (1993). Reflection-polarization pattern at water surfaces and correction of a common representation of the polarization pattern of the sky. *Naturwissenschaften*, *80*, 82–83.

Shaw, S. R. (1966). Polarized light responses from crab retinula cells. *Nature*, *211*, 92–93.

Ugolini, A., Talluri, P. & Vannini, M. (1989). Astronomical orientation and learning in the shrimp *Palaemonetes antennarius*. *Marine Biology*, *103*, 489–493.

Umminger, B. R. (1968). Polarotaxis in copepods: I. An endogenous rhythm in polarotaxis in *Cyclops vernalis* and its relation to vertical migration. *Biology Bulletin, 135*, 239–251.
Waterman, T. H. (1954). Polarization patterns in submarine illumination. *Science, 120*, 927–932.
Waterman, T. H. (1981). Polarization sensitivity. In Autrum, H. (Ed.), *Handbook of sensory physiology VII/6C* (pp. 281–469). Berlin: Springer.
Waterman, T. H. (1988). Polarization of marine light fields and animal orientation. *SPIE Vol. 925 Ocean Optics IX* (pp. 431–437).
Wehner, R. (1989). The hymenopteran skylight compass: matched filtering and parallel coding. *Journal of Experimental Biology, 146*, 63–85.

Acknowledgements—The financial support of the István Széchenyi Scholarship Foundation (Budapest) received by G. Horváth and a grant from the Deutsche Forschungsgemeinschaft to D. Varjú (SFB 307) are gratefully acknowledged.

APPENDIX A

Fresnel Formulae for Refraction Polarization of Light

When the electric field vector of incident light is parallel to the water surface, then the amplitude transmission coefficient of the air–water interface is

$$\sigma_{\parallel}(\theta_i) \equiv \frac{E_{\parallel}^{r}}{E_{\parallel}^{i}} = \frac{2n_a \cos\theta_i}{n_a \cos\theta_i + \sqrt{n_w^2 - n_a^2 \sin^2\theta_i}} \tag{A1}$$

where $E_{\parallel}^{i}$ and $E_{\parallel}^{r}$ are the electric field amplitudes of incident and refracted light, θ_i is the angle of incidence with respect to the vertical, n_a and n_w are the refractive indices of air and water (Guenther, 1990). When the incident electric field vector is perpendicular to the water surface, the amplitude transmission coefficient is

$$\sigma_{\perp}(\theta_i) \equiv \frac{E_{\perp}^{r}}{E_{\perp}^{i}} = \frac{2n_a n_w \cos\theta_i}{n_w^2 \cos\theta_i + n_a\sqrt{n_w^2 - n_a^2 \sin^2\theta_i}} \tag{A2}$$

where $E_{\perp}^{i}$ and $E_{\perp}^{r}$ are the electric field amplitudes of incident and refracted light (Guenther, 1990). In the general case, when the incident electric field vector E_i is oblique with respect to the water surface, the amplitudes of the parallel (horizontal) and perpendicular (vertical) components of the refracted electric field vectors are

$$\begin{aligned} E_{\parallel}^{r}(\theta_i, \varphi_i) &= \sigma_{\parallel}(\theta_i) E_i(\varphi_i)\sin\varphi_i, \\ E_{\perp}^{r}(\theta_i, \varphi_i) &= \sigma_{\perp}(\theta_i) E_i(\varphi_i)\cos\varphi_i \end{aligned} \tag{A3}$$

where φ_i is the direction of incident electric field vector measured from the vertical. The amplitude E_r and direction φ_r of the refracted electric field vector are

$$E_r[E_i(\varphi_i), \theta_i, \varphi_i] = E_i(\varphi_i)\sqrt{\sigma_{\parallel}(\theta_i)^2 \sin^2\varphi_i + \sigma_{\perp}(\theta_i)^2 \cos^2\varphi_i}, \tag{A4}$$

$$\varphi_r(\theta_i, \varphi_i) = \arctan\left[\frac{\sigma_{\parallel}(\theta_i)}{\sigma_{\perp}(\theta_i)} \tan\varphi_i\right]. \tag{A5}$$

The transmissivity for oblique linear polarization is

$$T(\theta_i, \varphi_i) = 1 - R = 1 - \rho_{\parallel}(\theta_i)^2 \sin^2\varphi_i - \rho_{\perp}(\theta_i)^2 \cos^2\varphi_i \tag{A6}$$

where R is the reflectivity, $\rho_{\parallel}(\theta_i)$ and $\rho_{\perp}(\theta_i)$ are the amplitude reflection coefficients (Guenther, 1990) for parallel and perpendicular polarization of incident light

$$\begin{aligned} \rho_{\parallel}(\theta_i) &= \frac{n_a \cos\theta_i - \sqrt{n_w^2 - n_a^2 \sin^2\theta_i}}{n_a \cos\theta_i + \sqrt{n_w^2 - n_a^2 \sin^2\theta_i}}, \\ \rho_{\perp}(\theta_i) &= \frac{n_w^2 \cos\theta_i - n_a\sqrt{n_w^2 - n_a^2 \sin^2\theta_i}}{n_w^2 \cos\theta_i + n_a\sqrt{n_w^2 - n_a^2 \sin^2\theta_i}}. \end{aligned} \tag{A7}$$

APPENDIX B

Refraction Polarization of Unpolarized Incident Light

When the incident light is unpolarized, then the degree of polarization δ_r of refracted light and the transmissivity T of the water surface (Guenther, 1990) are

$$\delta_r(\theta_i) \equiv \frac{E_r^{max2} - E_r^{min2}}{E_r^{max2} + E_r^{min2}} = \frac{\sigma_{\perp}(\theta_i)^2 - \sigma_{\parallel}(\theta_i)^2}{\sigma_{\perp}(\theta_i)^2 + \sigma_{\parallel}(\theta_i)^2}, \tag{B1}$$

$$T(\theta_i) = 1 - R(\theta_i) = 1 - \frac{\rho_{\parallel}(\theta_i)^2 + \rho_{\perp}(\theta_i)^2}{2}. \tag{B2}$$

APPENDIX C

Refraction Polarization of Partially Polarized Incident Skylight

Except for some special points of the sky (the neutral Arago, Babinet and Brewster points) the natural skylight is partially linearly polarized (Coulson, 1988). The polarization ellipse of skylight is described by the following expression

$$E_i(\varphi_i, \alpha_i, \epsilon_i) = \frac{E_i^{min}}{\sqrt{1 - \epsilon_i^2 \cos^2(\varphi_i - \alpha_i)}}, \quad E_i^{min} = E_i^{max}\sqrt{1 - \epsilon_i^2} \tag{C1}$$

where E_i^{min} and E_i^{max} are the half minor and major axes, α_i is the direction of the major axis with respect to the vertical plane of incidence, and

$$\epsilon_i = \sqrt{1 - \left[\frac{E_i^{min}}{E_i^{max}}\right]^2} \tag{C2}$$

is the excentricity of the ellipse. The relationships between the degree of polarization δ_i and excentricity ϵ_i are

$$\delta_i = \frac{\epsilon_i^2}{2 - \epsilon_i^2}, \quad \epsilon_i = \sqrt{\frac{2\delta_i}{1 + \delta_i}}. \tag{C3}$$

Combining equation (A4) and (C1), the electric field amplitude of partially polarized refracted skylight can be expressed as

$$E_r(\theta_i, \varphi_i, \alpha_i, \epsilon_i) = E_i^{min}\sqrt{\frac{\sigma_{\parallel}(\theta_i)^2 \sin^2\varphi_i + \sigma_{\perp}(\theta_i)^2 \cos^2\varphi_i}{1 - \epsilon_i^2 \cos^2(\varphi_i - \alpha_i)}}. \tag{C4}$$

The spatial distribution of the electric field vector of refracted light described by equation (C4) is not an ellipse but an oval. Therefore one must determine numerically the extrema E_r^{min} and E_r^{max} of function (C4) and then calculate the degree of polarization and direction of the major axis of the refraction polarization oval.

The transmissivity of the air–water interface for partially linearly polarized incident skylight is

$$T = 1 - R \equiv 1 - \frac{\int_0^{\pi} E_r^2(\varphi_i)\mathrm{d}\varphi_i}{\int_0^{\pi} E_i^2(\varphi_i)\mathrm{d}\varphi_i} = 1 - I\frac{\sqrt{1 - \epsilon_i^2}}{\pi},$$

$$I = \frac{\pi(\rho_{\parallel}^2 + \rho_{\perp}^2)}{2\sqrt{1 - \epsilon_i^2}} - \frac{\rho_{\parallel}^2 - \rho_{\perp}^2}{2}$$

$$\times \int_{-\infty}^{+\infty} \frac{1 - t^2}{\tau_4 t^4 + \tau_3 t^3 + \tau_2 t^2 + \tau_1 t + \tau_0}\mathrm{d}t,$$

$$\tau_0 = -\frac{\epsilon_i^2}{2}\cos(2\alpha_i), \quad \tau_1 = \tau_3 = -\epsilon_i^2 \sin(2\alpha_i),$$

$$\tau_2 = 2 - \epsilon_i^2, \quad \tau_4 = 1 - \epsilon_i^2 \sin^2\alpha_i. \tag{C5}$$

Since it is very complicated to calculate analytically integral I in equation (C5), the numerical integration is more expedient.

APPENDIX D

List of Symbols, their Meanings and Equation Numbers in the Appendices

Symbol	Meaning	Number of equations in Appendices
$n_a = 1.000$	Refractive index of air	(A1), (A2), (A7)
$n_w = 1.333$	Refractive index of water	(A1), (A2), (A7)
T	Transmissivity of the water surface	(A6), (B2), (C5)
$\sigma_\parallel$	Amplitude transmission coefficient of linearly polarized incident light, E-vector parallel to the water surface	(A1), (A3), (A4), (A5), (B1), (C4)
$\sigma_\perp$	Amplitude transmission coefficient of linearly polarized incident light, E-vector perpendicular to the water surface	(A2), (A3), (A4), (A5), (B1), (C4)
R	Reflectivity of the water surface	(A6), (B2), (C5)
$\rho_\parallel$	Amplitude reflection coefficient of linearly polarized incident light, E-vector parallel to the water surface	(A7), (B2), (C5)
$\rho_\perp$	Amplitude reflection coefficient of linearly polarized incident light, E-vector perpendicular to the water surface	(A7), (B2), (C5)
θ_i	Incident angle of light measured from the vertical	(A1), (A2), (A7)
$\theta_B = 53$ deg	Brewster angle; when $\theta_i = 53$ deg the reflected light is totally horizontally polarized	—
θ_s	Angular zenith distance of the sun	—
θ_s^a	Apparent angular zenith distance of the sun viewed from water through the Snell's window of the flat water surface	—
θ	Angular zenith distance of a celestial point observed from air	—
φ_i	Angle of obliqueness of the electric field vector of totally linearly polarized incident light measured from the vertical plane of incidence	(A3), (A4), (A5), (A6), (C1), (C4), (C5)
φ_r	Angle of obliqueness of the electric field vector of totally linearly polarized refracted light measured from the vertical plane of refraction	(A5)
φ	Angular azimuthal distance of a celestial point measured from the solar meridian	—
α_i	Direction of polarization of incident light measured from the vertical plane of incident	(C1), (C4), (C5)
α_r	Direction of polarization of refracted light measured from the vertical plane of refraction	—
λ	Wavelength of light	—
ϵ_i	Excentricity of the polarization ellipse of incident light	(C1), (C2), (C3), (C4), (C5)
δ_i	Degree of linear polarization of incident light	(C3)
δ_r	Degree of linear polarization of refracted light	(B1)
E_i	Amplitude of the electric field vector of incident light	(A3), (A4), (C1), (C5)
E_i^{max}	Maximum of E_i; half of the major axis of the polarization ellipse of incident light	(C1), (C2)
E_i^{min}	Minimum of E_i; half of the minor axis of the polarization ellipse of incident light	(C1), (C2), (C4)
$E_\parallel^i$	Horizontal (parallel to the water surface) component of E_i	(A1)
$E_\perp^i$	Vertical (perpendicular to the water surface) component of E_i	(A2)
E_r	Amplitude of the electric field vector of refracted light	(A4), (C4), (C5)
E_r^{max}	Maximum of E_r; half of the major axis of the RPO	(B1)
E_r^{min}	Minimum of E_r; half of the minor axis of the RPO	(B1)
$E_\parallel^r$	Horizontal (parallel to the water surface) component of E_r	(A1), (A3)
$E_\perp^r$	Vertical (perpendicular to the water surface) component of E_r	(A2), (A3)